Materials Research Proceedings 28 (2023) 429-436 https://doi.org/10.21741/9781644902479-47

Effects of cold-drawing and low-temperature annealing on the sensing properties of NiTi alloys

LI Yongji[1,a], LIN Jianping[1,2,b*], XIAO Yao[1,3,c] and MIN Junying[1,2,d]

[1]School of Mechanical Engineering, Tongji University, Shanghai, 201804, China

[2]Shanghai Key Laboratory for A&D of Metallic Functional Material, Tongji University, Shanghai 200092, China

[3]Institute for Advanced Study, Tongji University, Shanghai, 200092, China

[a]yongji@tongji.edu.cn, [b]jplin58@tongji.edu.cn, [c]xiaoy10@tongji.edu.cn, [d]junying.min@tongji.edu.cn

Keywords: NiTi Alloys, Cold-Drawing, Low-Temperature Annealing, Sensing Properties

Abstract. As an intelligent material, NiTi alloy exhibits shape memory effect and superelasticity. Its electrical resistance varies with deformation, thus making NiTi alloy a potential sensing material. Linearity and sensitivity are the two principal characteristics of sensors. Linearity reveals the deviation of the actual resistance-strain response from an ideal straight line and sensitivity is the change in input required to generate a unit change in output. Though conventional polycrystalline NiTi alloys possess high sensitivity and large strain range, the non-linear resistance-strain responses were not negligible thus hindering their sensing application. It was found that cold-drawing combing with low-temperature annealing had affected the linearity, while the influence rules were not clear. The electrical resistance of the fabricated NiTi alloy wires with various areal reductions were measured during stretching, and the results shown that the cold-drawn and annealed NiTi alloys exhibited better linearity though with decreased sensitivity. This investigation provides foundation for subsequent research on improving or tailoring the sensing properties of NiTi alloys.

Introduction

Shape memory alloys (SMAs), particularly NiTi alloys are special class of smart or intelligent materials gaining remarkable attention[1]. NiTi alloys possess the outstanding properties of shape-memory effect, superelasticity, high damping capacity as well as excellent wear resistance[2]. And they have been extensively applied in automotive, aerospace, mini actuators and micro-eletromechanical systems (MEMS).

Electric resistance is an important physical property of SMAs and it have been used to investigate the martensitic transformation, orientation, aging and plastic deformations[3]. Several researchers have noticed that changes in deformation are coupled to changes in electrical resistance of superelastic NiTi wires[4–6]. This relationship is of great importance because it makes NiTi a potential perception material, thus could further enrich its intelligent performance. Linearity and sensitivity are the two principal characteristics of sensors. The linearity is characterized by the non-linearity error, which is the maximum deviation of the change in the resistance from a specified straight line applied to the measured data points. The sensitivity is the ratio of change in the resistance to the strain. However, conventional polycrystalline shows a severer non-linear resistance-strain response, which hinders its sensing application.

The functional properties of NiTi are structure-sensitive, so they are possible to be improved by some process through creating well-developed structures. Lin et al. [7] fabricated three polycrystalline NiTi samples with different grain sizes from 35 nm to 110 nm and one crystalline-amorphous NiTi nanocomposite sample. They found that grain refinement and partial

amorphization can significantly improve the linearity of stress-strain response. Hua et al.[8] produced NiTi crystalline-amorphous nanocomposite by cold rolling with low-temperature annealing, which demonstrates near-linear superelasticity under stress of 2.3 GPa. Inspired by these strategies for improving its mechanical properties, we consider it practicable to change the electrical behaviors of NiTi by introducing amorphous structure. According to the preliminary results, it was found that cold-drawing combing with low-temperature annealing had affected the electrical behavior of NiTi alloy wires, while the influence rules were not clear.

The present work aims to investigate the effects of cold-drawing and low-temperature annealing on the sensing properties of NiTi alloy wires.

Materials and Experiments

Commercial superelastic NiTi wires with an initial diameter of 0.3 mm were purchased from PEIERTECH Incorporation (Jiangsu, China). The as-received nanocrystalline NiTi alloy wire was solution treated at 800 ℃ for 60 min in a muffle furnace and subsequently quenched by water.

Then the solution-treated samples were cold-drawn to thinner wires by continuous multi-pass processes using diamond dies without intermediate annealing. The die was lubricated with MoS_2 and the drawing speed was 300 mm/min. Due to the significant work hardening and cracking, it is difficult to lead the wires to pass through the die. And mechanical grinding is not applicable to make the wire end to a thinner diameter. Instead, a corrosion solution of HF: HNO_3: H_2O=1:5:20 by volume ratio was used to reduce the diameter of the wire end. According to the initial wire diameter of each drawing pass, the corrosion time varied from 5 min to 30 min. The summarized cold-drawing parameters including corrosion time, die diameter, pass or total areal reduction were listed in Table 1.

Table 1. Cold-drawing parameters of the NiTi wires.

Drawing Pass	Wire Diameter	Corrosion Time	Die Diameter	Pass Areal Reduction	Total Areal Reduction
1	0.3 mm	30 min	0.25 mm	30.6 %	30.6 %
2	0.25 mm	20 min	0.2 mm	36.0 %	55.6 %
3	0.2 mm	15 min	0.17 mm	27.8 %	67.9 %
4	0.17 mm	12 min	0.15 mm	22.1 %	75.0 %
5	0.15 mm	10 min	0.13 mm	24.9 %	81.2 %
6	0.13 mm	8 min	0.11 mm	28.4 %	86.6 %
7	0.11 mm	5 min	0.1 mm	17.4 %	88.9 %

The cold-drawn wires with final diameters of 0.2 mm, 0.15 mm, 0.1 mm (area reduction were 55.6 %, 75.0 %, 88.9 %, respectively) were then annealed at 300 ℃ for 60 min. As shown in Fig. 1, the tensile tests were executed on an MTS E44 testing machine with a loading and unloading rate of 5 mm/min at room temperature. The specimen elongation was measured via the crosshead travel monitor with resolution of 0.04 μm. The gauge length of the specimen was about 50 mm and the maximum elongation was 3 % with a strain rate of about $1.7 \times 10^{-3}\ /s$. The variations of electrical resistance were synchronously measured by a high precision multi-meter (GDM-8342, Good Will Instrument) with an accuracy of 0.1 %. The end of thin wire was clamped by three-jaw metal collet, and the electric cables of the multimeter were fixed on the collet by screws. For ensuring the NiTi wires insulate from the tensile machine, the collets were connected to the grip

holders with insulated handles. Both the crosshead travel distance and the measured electrical resistance were transferred to PC for further processing.

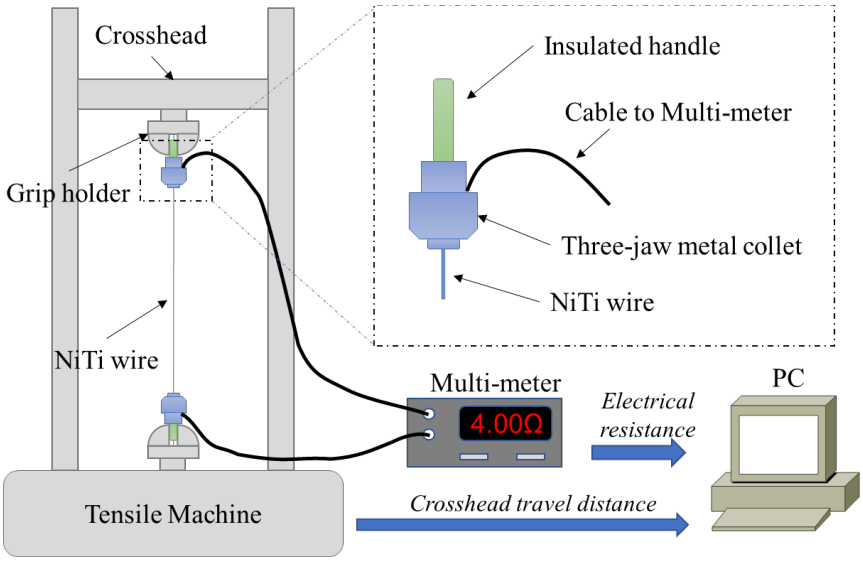

Fig. 1. Schematic diagram of the electrical resistance measurement.

Based on the measured data of electrical resistance and crosshead travel distance, the change ratio of resistance-strain curve is achieved. Through the least-squares method, the fitting line is achieved based on the experimental data. The calculation schematic of linearity and sensitivity is shown in Fig. 2. The sensitivity is defined as the slope of the fitting line, which is a unitless value. The linearity is characterized by the non-linearity error (NLE), which is calculated by Eq. 1.

$$NLE = \frac{\Delta_{max}}{Y_{max}} \times 100\% \, . \tag{1}$$

where Δ_{max} is the largest difference between the experimental data and the fitting line and Y_{max} is the largest change ratio of resistance.

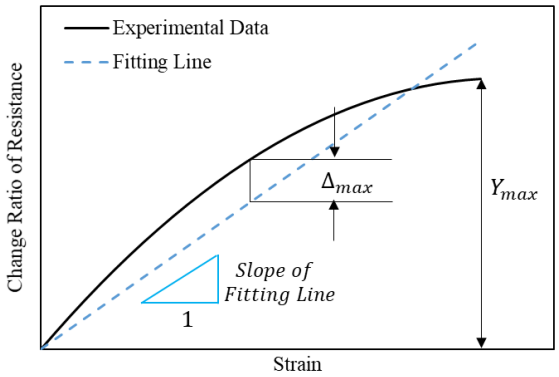

Fig. 2. Schematic diagram of the calculation of linearity and sensitivity.

According to the resistance formula (Eq. 2a and Eq. 2b), the electrical resistance is determined by two factors: the electrical resistivity (ρ) and size factor (L/S).

$$R_0 = \rho_0 * L_0/S_0 \, . \tag{2a}$$

$$R_\varepsilon = \rho_\varepsilon * L_\varepsilon / S_\varepsilon \,. \tag{2b}$$

where R is the measured resistance, ρ is the electrical resistivity, L is the length of the wire and S denotes the cross-sectional area of the specimen. The subscript 0 and ε stands for initial undeformed state and deformed state with a strain of ε, respectively.

From the constant volume assumption (Eq. 3a) [9] and the strain formula (Eq. 3b), the relative change ratio of electrical resistivity is inferred as Eq. 4.

$$L_\varepsilon * S_\varepsilon = L_0 * S_0 \,. \tag{3a}$$

$$L_\varepsilon = L_0 * (1 + \varepsilon) \,. \tag{3b}$$

$$\frac{detdet\,(\rho_\varepsilon)}{\rho_0} = \frac{\rho_\varepsilon - \rho_0}{\rho_0} = \frac{R_\varepsilon * {L_0}^2}{R_0 * {L_\varepsilon}^2} - 1 = \frac{R_\varepsilon - R_0 * (1+\varepsilon)^2}{R_0 * (1+\varepsilon)^2} \,. \tag{4}$$

Then assuming that the resistivity is constant, the relative change ratio of size factor is inferred as Eq. 5.

$$\frac{detdet\,(L_\varepsilon / S_\varepsilon)}{\frac{L_0}{S_0}} = \frac{L_\varepsilon/S_\varepsilon - \frac{L_0}{S_0}}{\frac{L_0}{S_0}} = (1+\varepsilon)^2 - 1 \approx 2\varepsilon \,. \tag{5}$$

To clarify the crystal structural change by cold-drawing and low-temperature annealing, Micro X-ray diffractometry (Micro-XRD) was carried out on Bruker D8 Advance using Cu-Kα radiation operated at 30 kV, 150 mA and a scanning speed of 4 °/min. A 2θ angle range from 5 ° to 85 ° was selected.

Results and Discussions

As shown in Fig. 3, the initial electrical resistivity exhibits a large variability in different NiTi alloy wires. The as-received NiTi alloy material possesses an initial electrical resistivity of 0.9 $\mu\Omega \cdot m$, which is higher by two orders of magnitude than common metal such as copper, aluminum. The resistivity of the cold-drawn NiTi (CD) increases significantly with the areal reduction. For the low-temperature annealed NiTi wires (CD+LTA), their resistivities maintain the same variation trend with the areal reduction but they decrease comparing with their cold-drawn counterparts. Notably, the electrical resistivities of the annealed NiTi wires with different areal reduction remain above that of the as-received.

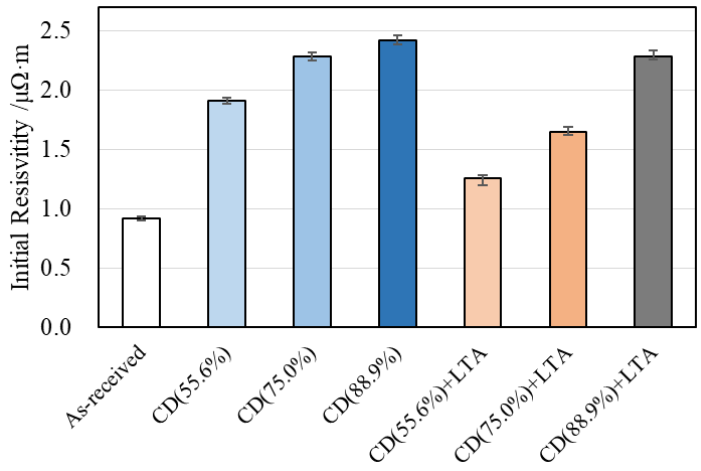

Fig. 3. The initial electrical resistivity of the NiTi alloy wires.

Materials Research Proceedings 28 (2023) 429-436 https://doi.org/10.21741/9781644902479-47

Fig. 4(a) displays resistance change ratio as a function of strain obtained during stretching of the as-received NiTi alloy wire and six tailored materials. The sensitivity and the non-linearity errors are summarized in Table 2. By comparing with the as-received sample, the cold-drawn and annealed NiTi wires demonstrates nearly linear resistance vs. strain relationship though with decreased sensitivity. With similar properties of linearity, the low-temperature annealed NiTi wires exhibited higher sensitivity than the cold-drawn ones.

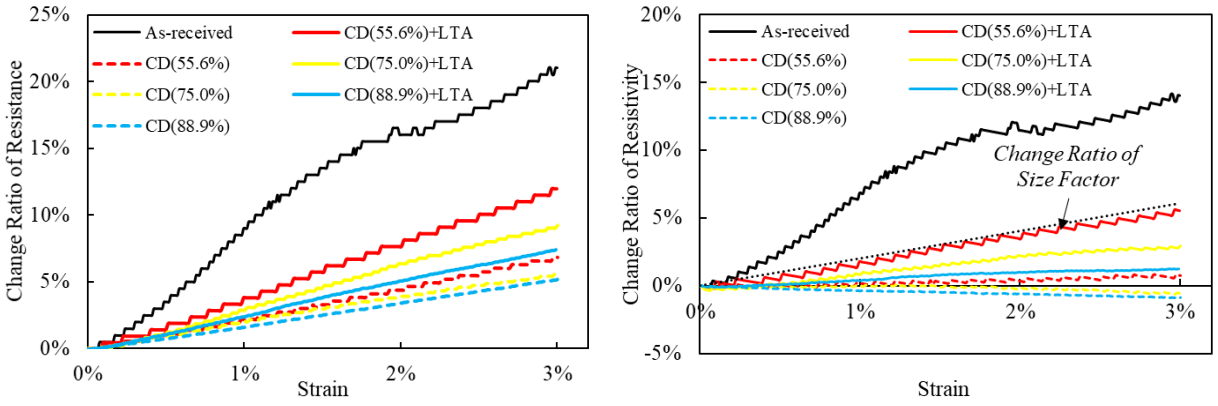

Fig. 4. (a) The resistance change ratio vs. strain curves and (b) the resistivity change ratio vs. strain curves of different NiTi alloy wires.

Table 2. Sensing sensitivities and non-linearity errors of different NiTi alloy wires.

Sample	Sensitivity	Non-Linearity Error
As-received	7.00	10.68 %
CD(55.6 %)	2.29	3.77 %
CD(75.0 %)	1.84	4.84 %
CD(88.9 %)	1.72	2.17 %
CD(55.6 %)+LTA	3.99	5.07 %
CD(75.0 %)+LTA	3.15	3.35 %
CD(88.9 %)+LTA	2.48	2.64 %

The factors of resistance variation were decoupled to the resistivity and the size factor. According to Eq. 5, the change ratio of size factor is only determined by strain and the slope is about 2. The resistivity change ratio vs. strain curves of different NiTi wires are shown in Fig. 4(b), in which the curve of size factor change ratio also added. For the as-received sample, the resistivity change ratio displays severe nonlinearity as well as a bigger slope than the size factor. The linearities of the tailored material are much better than the as-received one though the slopes are smaller. The slopes decrease with the areal reduction both for the cold-drawn and the annealed NiTi wires, while the latter ones are better than the former ones. Worth noting is that the resistivity change ratio becomes negative for the cold-drawn NiTi with 75.0 % or 88.9 % areal reduction and this issue will be discussed later.

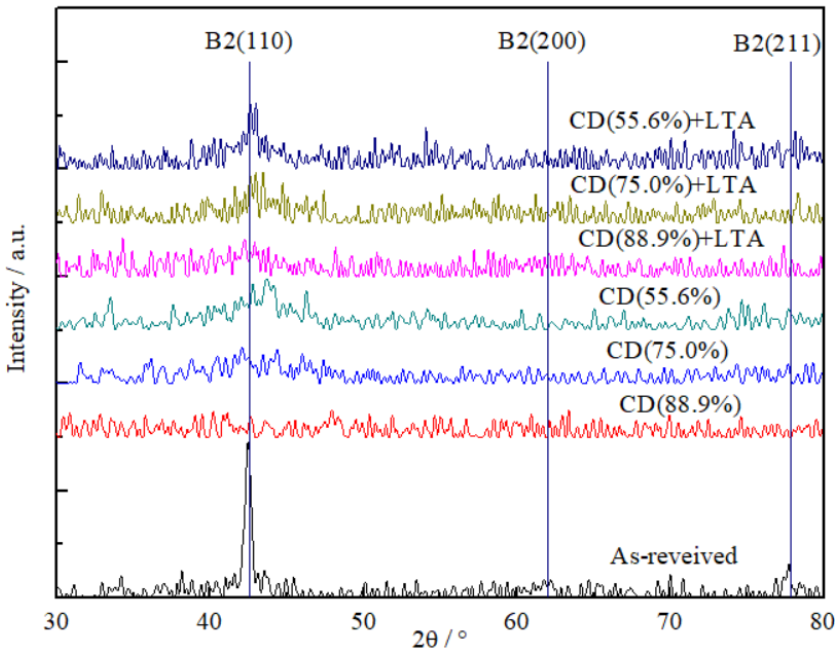

Fig. 5. Micro-XRD patterns of the as-received NiTi wire and six tailored ones.

Fig. 5 gives the Micro-XRD patterns of the different NiTi alloy wires. The Micro-XRD patterns of as-received wire shows that it is comprised of austenite phase (B2). There are marked drops in the intensity of the austenite peak for all of the cold-drawn wires and the low-temperature annealed wires. With the increasing of areal reduction, the intensities of the austenite peaks of both two kind of materials decrease, which illustrates that amorphization is intensified. The peak intensity of the annealed NiTi is higher than the cold-drawn one with the same areal reduction, which indicates that recrystallization of the austenite occurs to a certain extent in the low-temperature annealing processes.

According to the initial electrical resistivities and the Micro-XRD patterns, it suggests that cold-drawing leaded to amorphization of NiTi alloy and the amorphous phase rise with the increasing of areal reduction. In the subsequent low-temperature annealing, amorphous phase is subjected to recrystallization. For the as-received nanocrystalline NiTi material, elastic deformation appeared first in the stretching process and the stress-induced austenite-to-martensite transformation occurred when the strain exceeded about 1.5 %. The non-linear resistance-strain response is directly relevant to the stress-induced phase transformation. Ahadi and Sun [10] carried out in-situ tensile X-ray diffraction experiments for investigating the structure evolution during stress-induced transformation. NiTi alloy with a low B2 peak exhibited a continuous and smooth peak shift from B2 peak to B19'(Martensite) peak, while NiTi alloy with a higher peak displayer a sudden appearance of B19' peak. For the cold-drawn and the annealed NiTi wires, the containing amorphous phase suppresses the austenite-to-martensite transformation resulting in a continuous and smooth transformation, thus leading a more linear resistance-strain response.

Considering the negative slope of resistivity-strain response of the cold-drawn with great areal reduction (75.0 %, 88.9 %), it is assumed that the resistivity of pure amorphous phase is negative correlation with deformation. The amorphous phase is unstable and it can be subjected to crystallization under the stress [11]. The resistivity decreases in the crystallization process as the resistivity of crystal is lower than that of amorphous. Thus, there is a competitive relationship between crystalline and amorphous, which haves opposite effect on electrical resistivity of the deformed NiTi material. For CD 75.0 % and CD 88.9 %, the amount of amorphous is higher than other samples, so the amorphous phase plays a major role in resistivity variation resulting in a

negative slope. The changing sensitivity, i.e., the slopes of the resistance vs. strain curves, is attributed to the differences of amorphous phase content.

Summary

In this study, the effects of cold-drawing and subsequent low-temperature annealing on the sensing properties of NiTi alloy wires were investigated. The cold-drawn and annealed NiTi alloys exhibited better linearity though with smaller sensitivity. The greater areal reduction caused a better linearity. Combing with the initial electrical resistivities and the XRD patterns, it is inferred that amorphous phase is generated in NiTi alloy due to cold-drawing and low-temperature annealing. The amorphous phase suppresses martensitic transformation of the crystalline phase and consequently contributed to the improvement of linearity in the resistance-strain response.

Cold-drawing combining with low-temperature annealing is a practicable approach to regulate the sensing properties of NiTi alloys. For further investigations, the quantitative relationships between microstructures and sensing properties should be appealed.

Acknowledgments

This work was financially supported by National Natural Science Foundation of China (Grant No. 52075390).

References

[1] M. Sobczyk, S. Wiesenhütter, J.R. Noennig, T. Wallmersperger, Smart materials in architecture for actuator and sensor applications: A review, J. Intell. Mater. Syst. Struct. 33 (2022) 379-399. https://doi.org/10.1177/1045389X211027954

[2] N. Gangil, A.N. Siddiquee, S. Maheshwari, Towards applications, processing and advancements in shape memory alloy and its composites, J. Manuf. Process. 59 (2020) 205-222. https://doi.org/10.1016/j.jmapro.2020.09.048

[3] Y. Chen, O. Tyc, L. Kadeřávek, O. Molnárová, L. Heller, P. Šittner, Temperature and microstructure dependence of localized tensile deformation of superelastic NiTi wires, Mater. Des. 174 (2019) 107797. https://doi.org/10.1016/j.matdes.2019.107797

[4] S. Sławski, M. Kciuk, W. Klein, Change in Electrical Resistance of SMA (NiTi) Wires during Cyclic Stretching, Sensors 22 (2022) 3584. https://doi.org/10.3390/s22093584

[5] N. Michaelis, F. Welsch, S.-M. Kirsch, S. Seelecke, A. Schütze, Resistance monitoring of shape memory material stabilization during elastocaloric training, Smart Mater. Struct. 28 (2019) 105046. https://doi.org/10.1088/1361-665X/ab3d62

[6] A. Gurley, T.R. Lambert, D. Beale, R. Broughton, Dual measurement self-sensing technique of NiTi actuators for use in robust control, Smart Mater. Struct. 26 (2017) 105050. https://doi.org/10.1088/1361-665X/aa8b42

[7] H. Lin, P. Hua, Q. Sun, Effects of grain size and partial amorphization on elastocaloric cooling performance of nanostructured NiTi, Scripta Mater. 209 (2022) 114371. https://doi.org/10.1016/j.scriptamat.2021.114371

[8] P. Hua, M. Xia, Y. Onuki, Q. Sun, Nanocomposite NiTi shape memory alloy with high strength and fatigue resistance, Nat. Nanotechnol. 16 (2021) 409-413. https://doi.org/10.1038/s41565-020-00837-5

[9] M. Barati, S.A. Chirani, M. Kadkhodaei, L. Saint-Sulpice, S. Calloch, On the origin of residual strain in shape memory alloys: experimental investigation on evolutions in the microstructure of CuAlBe during complex thermomechanical loadings, Smart Mater. Struct. 26 (2017) 25024. https://doi.org/10.1088/1361-665X/aa5745

[10] A. Ahadi, Q. Sun, Stress-induced nanoscale phase transition in superelastic NiTi by in situ X-ray diffraction, Acta Mater. 90 (2015) 272–281. https://doi.org/10.1016/j.actamat.2015.02.024

[11] Y. Zhang, S. Jiang, M. Wang, Atomistic investigation on superelasticity of NiTi shape memory alloy with complex microstructures based on molecular dynamics simulation, Int. J. Plast. 125 (2020) 27-51. https://doi.org/10.1016/j.ijplas.2019.09.001